ADVANCED MATERIALS
www.advmat.de

Intrinsic Detectivity Limits of Organic Near-Infrared Photodetectors

Sam Gielen, Christina Kaiser, Frederik Verstraeten, Jonas Kublitski, Johannes Benduhn, Donato Spoltore, Pieter Verstappen, Wouter Maes, Paul Meredith, Ardalan Armin, and Koen Vandewal**

Organic photodetectors (OPDs) with a performance comparable to that of conventional inorganic ones have recently been demonstrated for the visible regime. However, near-infrared photodetection has proven to be challenging and, to date, the true potential of organic semiconductors in this spectral range (800–2500 nm) remains largely unexplored. In this work, it is shown that the main factor limiting the specific detectivity (*D) is non-radiative recombination, which is also known to be the main contributor to open-circuit voltage losses. The relation between open-circuit voltage, dark current, and noise current is demonstrated using four bulk-heterojunction devices based on narrow-gap donor polymers. Their maximum achievable *D** is calculated alongside a large set of devices to demonstrate an intrinsic upper limit of *D** as a function of the optical gap. It is concluded that OPDs have the potential to be a useful technology up to 2000 nm, given that high external quantum efficiencies can be maintained at these low photon energies.**

Near-infrared (NIR) light detection is key to an ever-growing demand for technical solutions in applications such as surveillance systems, facial recognition, industrial sorting and inspection, pulse oximetry, optical coherence tomography, and imaging.[1–10] Inorganic semiconductors like Ge, InGaAs, PbS, and HgCdTe allow for broadband light detection from 0.8 up to 10 µm with specific detectivities (*D**) near 10^{10} Jones or higher.[11] At the same time, some of those conventional materials contain toxic heavy metals and have a rather high overall production cost. Furthermore, commercial NIR imaging sensors have a limited resolution, related to the fact that the photoactive layer is mounted via wire-bonded electrical connections onto the silicon read-out integrated circuitry (ROIC).[12] This limits the smallest pixel pitch to approximately 10 µm since a very precise alignment between the ROIC and the active layer is required. To allow downscaling of the pixel size, an ongoing endeavor focuses on directly growing photoactive layers on the ROIC. However, device breakdown upon temperature fluctuations is often observed due to the difference in thermal expansion coefficients between the active layer and the ROIC or the electrical interconnects.[13] Another limit of conventional semiconductors is their broadband absorption. This makes wavelength selectivity only achievable by increasing device complexity, for example through additional optical filters and dichroic prisms, and poses extra limits on the spatial resolution.[14]

Given the intrinsic limitations mentioned above, innovation is likely to be material driven. Using sub-micrometer thick, strongly absorbing organic semiconductors, it is possible to decrease the pixel pitch to the diffraction limit of NIR light (around 4 µm) via monolithic integration.[11] Solution processing, combined with the fact that organic semiconductors are less brittle and more resistant to internal thermal stress, enables deposition of organic active layers directly on the ROIC, hereby severely simplifying device fabrication and lowering costs.[15] Furthermore, the absorption window of organic active materials can be fine-tuned via chemical modifications toward specific applications like bioimaging in the second NIR window (between 1000 and 1350 nm).[3,16] These advantages, as well as their non-toxicity, make organic semiconductors a hot topic in the NIR photodetection field.[17] A dozen NIR photoactive organic materials have been reported to date, with only a minor fraction

S. Gielen, F. Verstraeten, Dr. P. Verstappen, Prof. W. Maes, Prof. K. Vandewal
UHasselt – Hasselt University
Institute for Materials Research (IMO)
Agoralaan 1 – Building D, Diepenbeek 3590, Belgium
E-mail: koen.vandewal@uhasselt.be

S. Gielen, F. Verstraeten, Dr. P. Verstappen, Prof. W. Maes, Prof. K. Vandewal
IMEC
Associated Lab IMOMEC
Wetenschapspark 1, Diepenbeek 3590, Belgium

C. Kaiser, Prof. P. Meredith, Dr. A. Armin
Department of Physics
Swansea University
Singleton Park, Swansea SA2 8PP, UK
E-mail: ardalan.armin@swansea.ac.uk

J. Kublitski, Dr. J. Benduhn, Dr. D. Spoltore
Dresden Integrated Center for Applied Physics and Photonic Materials (IAPP) and Institute for Applied Physics
Technische Universität Dresden
Nöthnitzer Str. 61, Dresden 01187, Germany

The ORCID identification number(s) for the author(s) of this article can be found under https://doi.org/10.1002/adma.202003818.

© 2020 The Authors. Advanced Materials published by Wiley-VCH GmbH. This is an open access article under the terms of the Creative Commons Attribution License, which permits use, distribution and reproduction in any medium, provided the original work is properly cited.

The copyright line for this article was changed on 11 December 2020 after original online publication.

DOI: 10.1002/adma.202003818

showing photodetection up to 1400 nm.[18–21] Room-temperature values for D^* in this wavelength regime are in the order of 10^{10} Jones and hence one to two orders of magnitude below the performance of the inorganic variants in that wavelength range. Research on organic photodetectors (OPDs) therefore focuses on increasing D^*, while simultaneously targeting longer NIR wavelengths and maintaining other performance metrics.

D^* is negatively influenced by high noise levels and low photovoltaic external quantum efficiencies (EQE_{pv}).[22,23] Although narrow-gap organic materials absorbing up to 2 µm are known,[24–26] the often observed high dark (and noise) current is one of the major limiting factors, as it strongly increases with a decreasing optical gap.[27,28] While the effect of interfacial layers and traps on the dark and noise current has been elucidated, it is still unclear if under ideal circumstances, organic NIR detectors can reach similar performances as obtained with inorganic photodetectors.[29–31] No (thermodynamic) upper limit for D^* of organic NIR detectors has been rationalized and the longest achievable detection wavelength is still unknown.

In this work, four different NIR-photoactive narrow-gap donor polymers are investigated in a photodiode architecture and for the first time the open-circuit voltage (V_{OC}) is shown to be related to the dark current, noise current, noise equivalent power (NEP) and D^*. Specifically for these low E_{CT} systems the dark current is not dominated by the shunt current anymore, resulting in a quantitative relation between V_{OC} and dark current. This relation is generalized for previously reported organic NIR detectors and it is shown how, at low optical gaps, V_{OC} limits the ratio between light and dark current (I_{ph}/I_D). Applying the knowledge on the V_{OC} limits gathered in the organic solar cell field allowed us to calculate an upper limit for the D^* of 10^{12} and 10^{10} Jones at 1500 and 2000 nm, respectively. Moreover, it is found that D^* is predominantly limited by non-radiative losses, effectively decreasing D^* by 3 to 4 orders of magnitude in comparison to the background limited infrared photodetection (BLIP) for perfectly radiative materials.[11] Nonetheless, given the multiple advantages for commercialization, OPDs remain a viable alternative for the NIR regime up to 2 µm.

Photodetectors are often photovoltaic-based and are made in some form of diode architecture, operated in the reverse direction. In the ideal case, the total current flowing through the device under illumination is described by the Shockley equation:

$$I = I_0\left(e^{qV/kT} - 1\right) - I_{ph} \tag{1}$$

with q being the elementary charge and k the Boltzmann constant. At a temperature T, the total current I depends on the dark saturation current I_0, the photocurrent I_{ph} and the applied voltage V. In the dark, $I = I_D$ and $I_{ph} = 0$, and Equation (1) can be written as:

$$I_D = I_0\left(e^{qV/kT} - 1\right) \tag{2}$$

For negative voltages, the diode current from Equation (1) approaches the dark saturation current ($I_D \to -I_0$). I_0 is considered the "thermodynamic equilibrium recombination current", due to thermally activated band to band transitions as described by Cuevas.[32] However, due to the presence of traps, pinholes, shunts, or charge-carrier injection from the contacts, in a real diode I_D is typically well above I_0 and is dominated by the strongest recombination mechanism, which could stem from trap-assisted recombination described by Shockley–Read–Hall statistics.[33] In what follows, it is assumed for simplicity that at sufficiently small bias voltages, where series resistance can be neglected, those additional currents are described by I_{shunt}. I_D is therefore expressed as:

$$I_D = I_0\left(e^{qV/kT} - 1\right) + I_{shunt} \tag{3}$$

where $I_{shunt} = V/R_{shunt}$ and R_{shunt} is the shunt resistance. In the literature, it was shown that I_{shunt} can be suppressed using interlayers, thick junctions, and an optimized device architecture.[34–36] Moreover, in the case of bulk heterojunctions (BHJs) with a low effective bandgap, I_0 can be high in comparison to I_{shunt}, since I_0 was previously found to scale with the effective bandgap.[37,38] Importantly, because of the presence of shunts, I_0 is experimentally often difficult to access. However, when R_{shunt} is sufficiently high, the ratio of I_{ph}/I_0 relates to the V_{OC} of the solar cell. Indeed, an expression for the V_{OC}

$$V_{OC} = \frac{kT}{q}\ln\left(\frac{I_{ph}}{I_0} + 1\right) \tag{4}$$

can be derived by considering that at open circuit ($V = V_{OC}$), the dark current given by Equation (3) equals the photocurrent I_{ph}, which is considerably higher than I_{shunt}. This establishes a relation between V_{OC} and I_{ph}/I_0.

In order to verify the above relations, four narrow-gap polymers are used as donors in combination with $PC_{71}BM$ as acceptor in BHJ photodiodes of the structure glass/ITO/ZnO-PEIE/active layer/MoO_3/Ag. The synthesis and performance in NIR photodiodes of three of the used polymers—PTTBAI, PBTQ(OD), and PTTQ(HD)—have been reported before.[16,39] The synthesis route for the novel ultralow gap push–pull copolymer PTTQn(HD) is provided in the Supporting Information (Scheme S1, Supporting Information). The chemical structures and their frontier orbital energy levels, as estimated via cyclic voltammetry (CV, Figure S2, Supporting Information), are shown in **Figure 1**a–b, respectively. The donor polymers are characterized by a low LUMO energy level, which results in low optical gaps for the polymers (<1.5 eV, Figure S3, Supporting Information) and effective gaps (charge transfer energy, E_{CT}) below 1.12 eV for the BHJs.

Given these effective gaps (between 0.81 and 1.12 eV), low V_{OC} values between 0.12 and 0.44 V are obtained under high intensity radiation (100 mW cm^{-2}), in accordance to the previously reported linear relationship between E_{CT} and V_{OC}.[40] For such low effective gaps, it is expected that I_0 becomes comparable or higher than I_{shunt}, which makes Equation (3) and (4) suitable for relating the dark currents at reverse voltages to V_{OC}.

A fit to the dark current for the devices based on the four material systems shown in Figure 1 is attempted using Equation (3) and returning R_{shunt} and I_0 as fit parameters, as shown in Figure S4, Supporting Information. This approach is indeed only useful when I_0 is not much smaller than I_{shunt}, a requirement that is only met in narrow-gap systems with very high film quality to minimize the shunt effects. The fit parameters, R_{shunt} and I_0, are summarized in Table S1, Supporting Information.

© 2020 The Authors. Advanced Materials published by Wiley-VCH GmbH

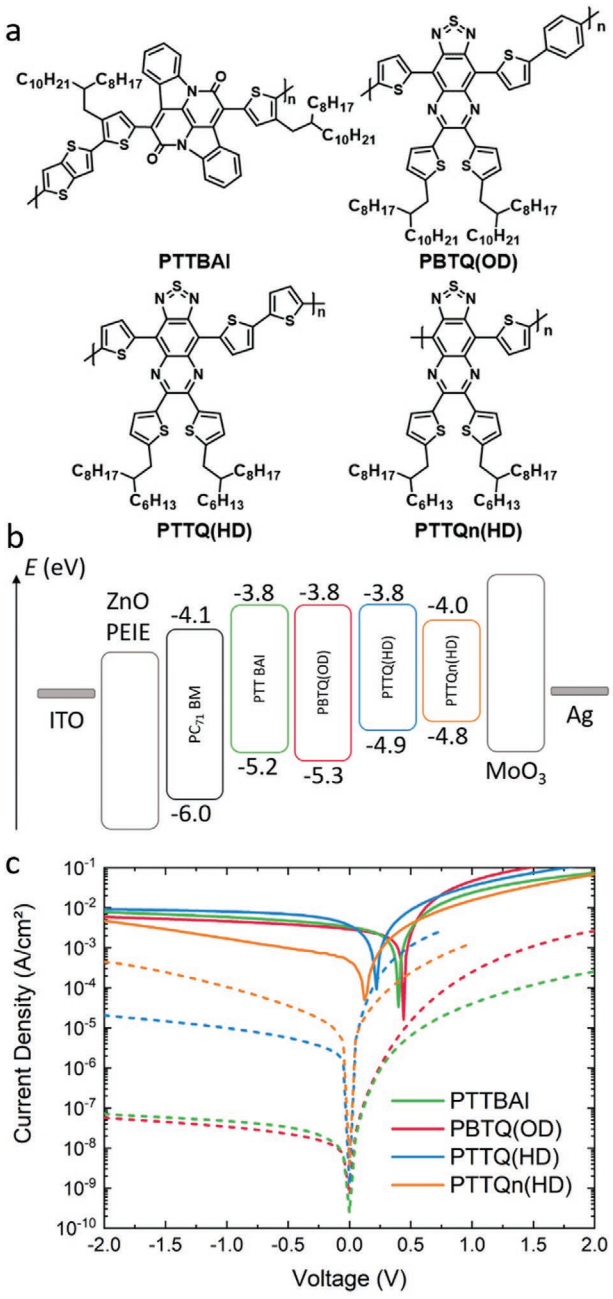

Figure 1. a) Chemical structures of the four NIR absorbing donor copolymers. b) Energy level diagram displaying the different layers used in the inverted OPD device stack. The frontier orbital energy levels are estimated by CV. c) *J*–*V* curves for the OPD devices (solid lines: light current under 1 sun illumination; dashed lines: dark current).

Importantly, at small reverse bias (≤ –0.1 V), the contribution of I_{shunt} can be neglected and hence the experimental I_D equals I_0, except for the PTTQn(HD). Excluding PTTQn(HD), we therefore expect close agreement between the V_{OC} calculated using I_0 in Equation (4) and the experimental V_{OC}. Table S1, Supporting Information, shows that both are on average 0.05 V apart, while the largest offset is observed for PBTQ(OD) with 0.09 V.

The experimental V_{OC} and the ratio I_{ph}/I_D are therefore expected to be logarithmically related when I_D is evaluated at a sufficiently low reverse voltage. Indeed, as shown in **Figure 2**a for the four studied material blends, as well as for a large set of reported BHJs (additional information in Table S2 and Figure S5, Supporting Information), a linear relation between V_{OC} and I_{ph}/I_D on a semi-logarithmic scale is observed for V_{OC} < 0.25 V. Since I_D is always larger than I_0, the points in Figure 2a are either very close to the intrinsic limit (within the experimental error) or well above, but cannot be significantly below. For V_{OC} < 0.25 V, the experimentally measured dark current is limited to $I_D < 25 \times I_0$. For higher voltages, I_{ph}/I_D increasingly deviates from the intrinsic limit, due to the increasing contribution of I_{shunt}. For V_{OC} = 1 V,

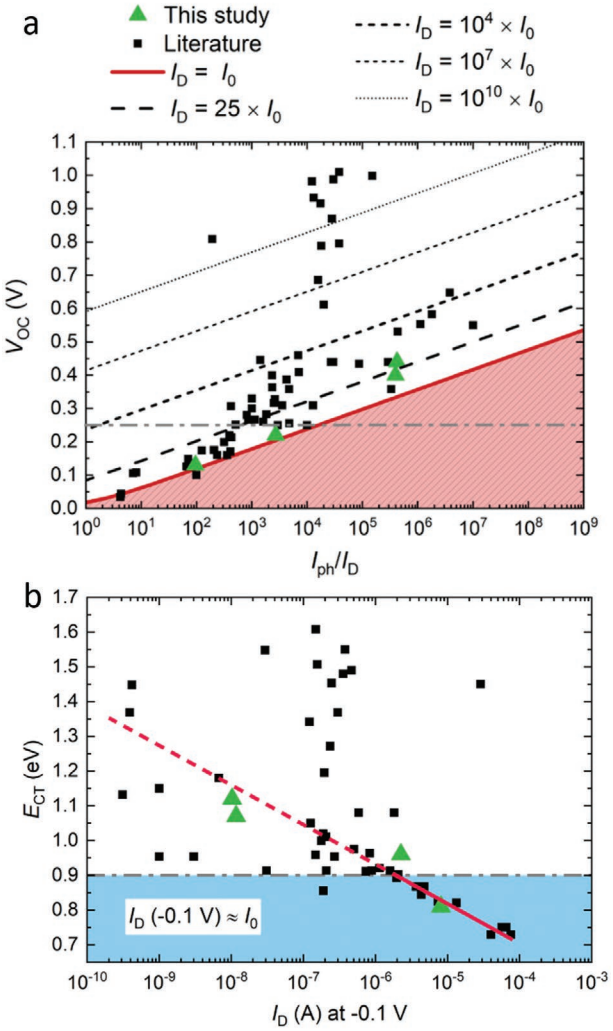

Figure 2. a) Calculated ratio of I_{ph} to I_D plotted against the experimental V_{OC} on a semi-logarithmic scale. The green symbols represent the narrow-gap donor polymers and the respective devices studied in this work, while the black symbols represent a large set of reported BHJs (all fullerene-based devices, additional information in Table S2, Supporting Information). The red solid line marks the lower thermodynamic limit of the dark current. b) I_D (at –0.1 V) as a function of E_{CT} for the devices studied in this work (green symbols) and the reported BHJs (black symbols). For devices with V_{OC} < 0.25 V and E_{CT} < 0.9 V (which agrees with the offset typically observed between V_{OC} and E_{CT}/q in organic BHJs of around 0.6 to 0.7 V), I_D is close to I_0 if the device structure is optimized. The red solid line marks the region in which I_D(–0.1 V) ≈ I_0. In the region of the red dashed line, no correlation between E_{CT} and I_D (–0.1 V) is found.

© 2020 The Authors. Advanced Materials published by Wiley-VCH GmbH

I_D is typically 12 orders of magnitude higher than I_0. Note that the I_D used in Figure 2a,b was taken at –0.1 V for all BHJs to reduce the influence of additional shunt currents. However, if devices are not fully optimized and hence show some leakage, I_{ph}/I_D cannot be close to the intrinsic limit set by the V_{OC}.

In agreement with previous literature, a linear relationship between E_{CT} and I_D is observed, but only for $E_{CT} < 0.9$ eV, as shown in Figure 2b. This agrees with V_{OC} values up to 0.25 V, since the offset observed between the V_{OC} and the E_{CT}/q in organic BHJs is typically around 0.6–0.7 V. From the trend shown in Figure 2b, the minimum achievable I_D can be estimated for a given material system with known E_{CT}. Moreover, it confirms that the fitting procedure of extracting I_0 from I_D is reasonable only in the case of low E_{CT} BHJs. From the above it is clear that the lowest achievable dark current, I_0, at reverse voltages is set by the V_{OC}. Devices with an E_{CT} and optical gap smaller than 0.9 eV (≈1380 nm) approach this limit.

So far, it is shown that for a BHJ with a characteristic E_{CT} and V_{OC}, there is a theoretical upper limit for the ratio I_{ph}/I_D that decreases with decreasing V_{OC} (E_{CT}). It is clear that efficient photodetection can only be achieved when the ratio I_{ph}/I_D is high. Below, we demonstrate how this relates to upper limits of photodetector performance, which is described by its specific detectivity D^*. The experimental D^* is either obtained from the ratio of responsivity (R) to noise current (i_{noise}) according to

$$D^* = \frac{R\sqrt{A\Delta f}}{i_{noise}} \tag{5a}$$

or directly from the NEP via

$$D^* = \frac{\sqrt{A\Delta f}}{\mathrm{NEP}} \tag{5b}$$

Note that D^* is always normalized to the square root of the area (A) multiplied by the bandwidth (Δf).[41] To obtain D^* according to Equation (5a), R is first calculated from the measured EQE_{pv} (Figure S6 and S7, Supporting Information) at –2, –1, and 0 V according to $R = EQE_{pv} \cdot \lambda/1240$. Secondly, i_{noise} is measured at different bias using a spectrum analyzer (spectra shown in Figure S8, Supporting Information). In this way, a spectrum of D^* is obtained as shown in **Figure 3**b for PBTQ(OD) and in Figure S9, Supporting Information, for the other materials investigated in this study. However, the above assumes that the current response of the device will decrease linearly with light power until it vanishes in the current noise. To verify this assumption, a second method is used to obtain D^* directly from the NEP (Equation (5b)) at a single wavelength (520 nm) by gradually decreasing the light power and measuring the respective current. A graphical representation is shown in Figure S10, Supporting Information, for two photodiodes demonstrating a linear dynamic range over 9 orders of magnitude for the PBTQ(OD) based device. Both methods are found to be in good agreement, since D^* values obtained from Equation (5a) and (5b) differ only by a factor of 1.6 and 2.6 for PBTQ(OD) and PTTBAI, respectively (Figure S11, Supporting Information).

With an accurate determination of the experimental D^* at hand, we can now consider upper limits of D^*. To do so, i_{noise} is decomposed into different noise sources, such as shot noise (i_{shot}), thermal noise ($i_{thermal}$), and flicker noise.[42] Shot noise is due to the randomness of the emission of electrons and hence linearly proportional to the current magnitude,

$$\left\langle i_{shot}^2 \right\rangle = 2qI\Delta f \tag{6}$$

Thermal noise depends on the total parallel resistance R_P, including R_{shunt} (more information is provided in the Supporting Information) and effective diode resistance at zero bias voltage according to

$$\left\langle i_{thermal}^2 \right\rangle = \frac{4kT}{R_p}\Delta f \tag{7}$$

While shot and thermal noise are considered white noise, flicker noise is frequency dependent in the low frequency regimes, as shown in Figure S8, Supporting Information. To minimize the influence of the flicker noise, an experimental frequency range between 1 and 3 kHz was chosen, and therefore the total noise current can be described as

$$i_{noise} = \sqrt{\left\langle i_{shot}^2 \right\rangle + \left\langle i_{thermal}^2 \right\rangle} \tag{8}$$

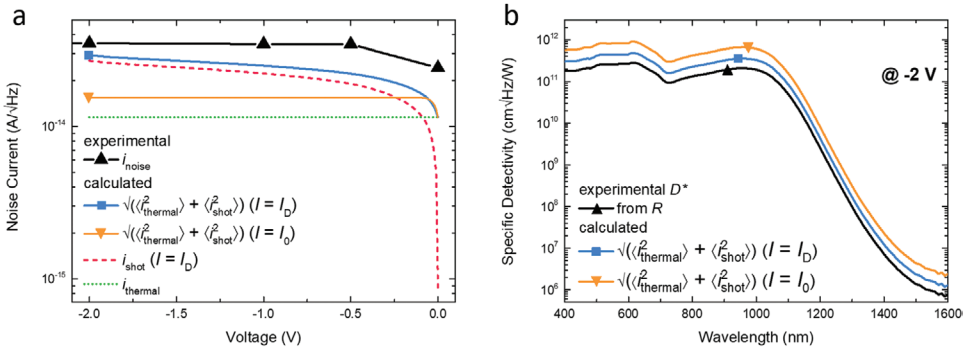

Figure 3. a) Calculated and experimental noise currents for a photodiode based on PBTQ(OD). The experimental noise current (black marker) is at least twice the noise current calculated from the measured dark current (blue marker) or from the dark saturation current (orange marker). Below –0.1 V, the total calculated noise current is dominated by shot noise (red dashed line), and above –0.1 V by thermal noise (green dashed line). b) The specific detectivity of a photodiode with PBTQ(OD) calculated using different levels of noise current (same marker notation as for Figure 3a). For the calculation, the responsivity and noise current at –2 V were considered.

© 2020 The Authors. Advanced Materials published by Wiley-VCH GmbH

Figure 3a shows the experimental i_{noise} alongside the calculated noise current using Equation (8) for the photodiode based on PBTQ(OD) (see Figure S12, Supporting Information, for the other donor materials). Note that the thermal noise becomes dominant at lower magnitudes of the reverse voltage, here for $|V| < 0.1$ V. Moreover, the experimental i_{noise} is expected to be above the calculated one since Equation (8) does not account for all noise sources (which are known to exist but not well described) and experimental limitations imposed by the amplifier noise. Consequently, the experimental D^* is expected to be lower than the calculated one according to Equation (5a).

First, we use Equation (6) and assume that $I = I_D$ to calculate i_{noise}, which is subsequently used in Equation (8) to obtain D^*. I_D is taken from the dark current–voltage (I–V) characteristics as shown in Figure 1c. This procedure of obtaining D^* is often encountered in literature in the absence of experimental noise current spectra as well as in neglection of $i_{thermal}$.[18,43] As a result, D^* is often overestimated, as shown in Figure 3b.

In contrast, when i_{noise} is calculated according to Equation (6) assuming $I = I_0$, the resulting upper limit of D^* for the photodiode with PBTQ(OD) is only 3.2 times higher than the experimentally determined D^* across the spectrum. Herein, I_0 was obtained from the fittings to the dark I–V characteristics, as described earlier. Hence, for this material system, it is clear that the device architecture is well optimized, since it is working close to the limit of D^* imposed by the active layer blend and its V_{OC}.

The above analysis shows that at a given responsivity R, the maximum D^* is reached when $I_D = I_0$, of which the lower limit is set by the V_{OC}. In accordance to Equation (5a), D^* can be further increased if R can be increased. In the Supporting Information, an expression is derived, using the relationship between I_{ph} and R, in which D^* is proportional to $I_{ph}/\sqrt{I_0}$. As I_0 is limited by the V_{OC}, known factors preventing the V_{OC} being closer to the optical gap in organic BHJs will also affect the maximum achievable D^*. This is further explored in the next paragraph.

From previous work, it is known that V_{OC} losses are intrinsic to organic BHJs due to the radiative and non-radiative recombination of charge carriers.[40,44] The dark saturation current comprises a radiative contribution $I_{0,R}$ and a non-radiative contribution $I_{0,NR}$. $I_{0,R}$ can be calculated via

$$I_{0,R} = q\int_0^\infty \mathrm{EQE}_{pv}(E)\,\varphi_{BB}(E)\,dE \tag{9}$$

where $\varphi_{BB}(E)$ is the temperature dependent black body spectrum. In order to calculate upper limits for D^*, $I_{0,R}$ is calculated using Equation (9) for a perfect photodiode with a step-like EQE_{pv}, that has its maximum value of 1 for energies above the E_{CT} and 0 below. By taking only the shot noise component of $I_{0,R}$ into account, D^* is calculated via Equation (5a). The respective D^* spectrum belongs to a so-called background limited infrared photodetector (BLIP; derivation shown in the Supporting Information), where the only source of current noise corresponds to the shot noise of the photocurrent induced by thermal radiation.[12] **Figure 4**b shows the background limited D^* at 300 K for different optical gap energies corresponding to wavelengths up to 2 µm. By lowering the optical gap, D^* decreases down to 5×10^{13} Jones at 2 µm, which marks the thermodynamic limit of D^* for any type of photodetector without photo-multiplicative gain ($EQE_{pv} \leq 1$). For organic BHJs, the EQE_{pv} is below 1 and has a strong spectral dependence as well as sub-gap features, which will increase $I_{0,R}$ in comparison to the step-like EQE_{pv} example and hence decrease D^*. Furthermore, it is known that for organic BHJs, the total dark saturation current is dominated by the non-radiative component $I_{0,NR}$. A realistic upper limit for the achievable D^* for organic NIR

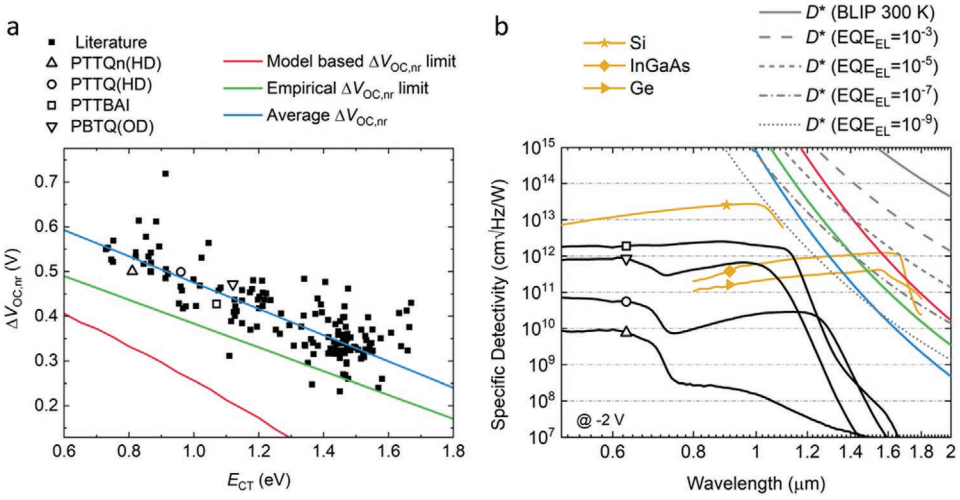

Figure 4. a) $\Delta V_{OC,NR}$ as a function of E_{CT} for BHJs studied in this work (hollow symbols) and literature-reported BHJs (black squares).[40] The red line represents a model based lower limit,[45] the green line shows a previously reported[40] empirical lower limit to $\Delta V_{OC,NR}$ and the blue line shows an average value for $\Delta V_{OC,NR}$ as observed in this study. b) Specific detectivity as a function of wavelength. The black lines represent the D^* for BHJs studied in this work using the same symbols as in Figure 4a. The upper limit of the D^* is calculated for different contributions of non-radiative recombination currents (represented as EQE_{el} values according to Equation (10)) to the dark current ranging from zero (solid grey line: BLIP at 300 K) to very high ($EQE_{el} = 10^{-9}$). The colored lines represent the upper limit of the D^* determined from the models used in Figure 4a. The D^* of commercial photodetectors (orange lines) are added for comparison.[47]

© 2020 The Authors. Advanced Materials published by Wiley-VCH GmbH

Table 1. Device performance parameters for the photodiodes with the studied donor materials.

Material	V_{OC} [V]	$I_{0,R}$ [A][a)]	EQE_{el}[b)]	$\Delta V_{OC,NR}$ [V][c)]	E_{CT} [eV][d)]
PTTBAI	0.40	5.59×10^{-16}	6.54×10^{-8}	0.42	1.07
PBTQ(OD)	0.44	8.54×10^{-17}	1.18×10^{-8}	0.47	1.12
PTTQ(HD)	0.22	4.60×10^{-15}	4.10×10^{-9}	0.49	0.96
PTTQn(HD)	0.12	3.65×10^{-15}	3.86×10^{-9}	0.49	0.81

[a)]Calculated from Equation (9); [b)]Calculated from Equation S9, Supporting Information (more detailed description in Supporting Information); [c)]Calculated from Equation (10) (more detailed description in Supporting Information); [d)]E_{CT} values obtained from the intercept of the reduced EQE_{pv} and EL spectrum (Figure S13, Supporting Information).

OPDs can therefore be obtained by considering $I_{0,NR}$ and a box-shaped EQE_{pv} that is 1 for energies above E_{CT}, as will be shown below.

In the radiative limit ($I_0 = I_{0,R}$), the upper limit of the V_{OC} ($V_{OC,R}$) is obtained via Equation (4). The difference between $V_{OC,R}$ and the experimental V_{OC} equals the non-radiative voltage losses ($\Delta V_{OC,NR} = V_{OC,R} - V_{OC}$). Figure 4a shows $\Delta V_{OC,NR}$ for a large set of BHJs with different E_{CT}, including the devices studied here. Clearly, $\Delta V_{OC,NR}$ depends on E_{CT}. An increase of $\Delta V_{OC,NR}$ by 300 mV is observed when E_{CT} decreases from 1.6 to 0.8 eV. As a next step, $I_{0,NR}$ is obtained from $\Delta V_{OC,NR}$ via

$$\Delta V_{OC,NR} = \frac{kT}{q} \ln\left(EQE_{el}^{-1}\right) \quad (10)$$

where $EQE_{el}^{-1} = \frac{I_{0,R} + I_{0,NR}}{I_{0,R}}$.[45,46] **Table 1** summarizes the device parameters related to non-radiative losses for the devices studied in this work. Since $I_{0,NR} \gg I_{0,R}$, the dark saturation current will be dominated by the non-radiative recombination current and it can be assumed that $I_0 = I_{0,NR}$.

Subsequently, D^* is calculated under consideration of non-radiative recombination currents that are unavoidable in organic BHJs. First, $I_{0,NR}$ is considered to be independent of E_{CT} and thus constant across the spectrum and corresponding to realistic EQE_{el} values between 10^{-3} to 10^{-9}. As shown in Figure 4b, D^* decreases by one order of magnitude across the spectrum for a decrease of EQE_{el} by two orders of magnitude (corresponding to an increase of $I_{0,NR}$ by two orders).

Recent reports have identified high frequency molecular vibrations as the source of the rather large non-radiative decay rates in organic BHJs,[40] explaining the previously experimentally observed dependence of $I_{0,NR}$ on E_{CT}. Below, we distinguish three different cases for $\Delta V_{OC,NR}$ as a function of E_{CT}: i) a model-based lower limit for $\Delta V_{OC,NR}$ reported by Azzouzi et al. (in which high and low frequency vibrational modes, 150 and 50 meV, respectively, are considered to be low for organic semiconductors, hence providing a lower limit for the non-radiative voltage losses),[45] ii) an empirical lower limit for $\Delta V_{OC,NR}$ reported by Benduhn et al.,[40] and iii) an average value for $\Delta V_{OC,NR}$ as a function of E_{CT} as observed in this study. While case (i) predicts an upper limit for D^* to about 10^{10} Jones at 2 µm, the empirical and average cases (ii) and (iii) predict that OPDs based on materials with similar recombination properties as the ones found in current BHJs will typically not reach more than 10^9 Jones at 2 µm. At the same time, we expect D^* to reach a respectable 10^{12} Jones at 1500 nm if the EQE_{pv} can approach 1. This value is comparable to commercial InGaAs detectors and even surpasses commercial Ge detectors (Figure 4b).[47] Importantly, the upper limit of D^* decreases significantly faster for models where $I_{0,NR}$ is dependent on E_{CT} than if it is not. Hence, further red-shifting the absorption to the mid-infrared (2–10 µm) in OPDs is not expected to be useful, as it seems impossible to compete with inorganic alternatives. Nonetheless, OPDs remain a viable alternative for the NIR regime up to 2 µm, given that EQE_{pv} values approaching 1 can be achieved at such low gaps with a steep EQE_{pv} tail onset.

In a recent study, Wu et al. reported on an upper limit for D^* that is around a 100 times higher at 2 µm than calculated here.[48] Their model considers as a limit to D^* the effect of tail-state broadening on noise related to thermally activated charge generation and recombination over the effective bandgap. Here, we follow a different approach and considered the non-radiative dark saturation current as a more important limiting factor. This dark mechanism has been shown to be present in both non-fullerene acceptor (NFA) containing and NFA free BHJs, and results, as compared to Ref. [48], in a stronger increase in the noise current toward longer wavelengths.[40]

To increase D^* to the theoretical maximum for NIR organic photodiodes, as indicated by the red curve in Figure 4b, one should find a way to decrease $\Delta V_{OC,NR}$ while maintaining the NIR absorption. A reasonable pathway could be the use of NFA materials as these are known to yield lower non-radiative V_{OC} losses.[49,50] A hurdle to overcome is to find a well-performing combination of a NIR-photoactive donor and NFA, as only a selected group of donor materials tend to work well with the best NFAs produced to date.[51]

In this work, the intrinsic limit of the specific detectivity of NIR organic photodiodes was determined. For narrow-gap donor polymers combined with fullerene acceptors, the open-circuit voltage was related to the dark current, noise current, and specific detectivity. For devices with open-circuit voltages up to 0.25 V under 100 mW cm^{-2} illumination, corresponding to effective and optical gaps lower than 0.9 eV, it is found that the experimental dark current approaches its theoretical limit. Above 0.25 V, the deviation increases with increasing open-circuit voltage. Moreover, it is observed that the upper limit for the D^* of NIR OPDs is predominantly limited by non-radiative losses, effectively decreasing D^* by 3 to 4 orders of magnitude in comparison to the BLIP for perfectly radiative materials. This allowed to calculate an intrinsic upper limit for D^* of 10^{12} and 10^{10} Jones at 1500 and 2000 nm, respectively. The applicability of OPDs to the NIR region above 2 µm seems therefore

© 2020 The Authors. Advanced Materials published by Wiley-VCH GmbH

negligible and future research should focus on reducing voltage losses, in which NFAs will likely play an important role.

Supporting Information

Supporting Information is available from the Wiley Online Library or from the author.

Acknowledgements

S.G. and C.K. contributed equally to this work. S.G. and F.V. acknowledge the Research Foundation – Flanders (FWO Vlaanderen) for granting them a PhD fellowship. P.V. is a postdoctoral fellow of the FWO. K.V. and W.M. are grateful for project funding by the FWO (G0D0118N, G0B2718N, and GOH3816NAUHL) and the European Research Council (ERC, grant agreement 864625). Hasselt University and IMOMEC have been partners in the SBO project MIRIS (Monolithic Infrared Image Sensors), supported by VLAIO (Vlaams Agentschap Innoveren en Ondernemen). C.K. is recipient of a UKRI EPSRC Doctoral Training Account studentship. P.M. is a Sêr Cymru II Research Chair and A.A. a Rising Star Fellow funded through the Welsh Government's Sêr Cymru II "Sustainable Advanced Materials" Program (European Regional Development Fund, Welsh European Funding Office and Swansea University Strategic Initiative). J.K. acknowledges the German Academic Exchange Service (DAAD) for the PhD fellowship. J.B. acknowledges the Sächsische Aufbaubank through project no. 100325708 (Infrakart).

Conflict of Interest

The authors declare no conflict of interest.

Keywords

near-infrared, non-radiative losses, organics, photodetectors, specific detectivity

Received: June 4, 2020
Revised: September 18, 2020
Published online: October 19, 2020

[1] R. D. Jansen-van Vuuren, A. Armin, A. K. Pandey, P. L. Burn, P. Meredith, *Adv. Mater.* **2016**, *28*, 4766.
[2] S. Park, K. Fukuda, M. Wang, C. Lee, T. Yokota, H. Jin, H. Jinno, H. Kimura, P. Zalar, N. Matsuhisa, S. Umezu, G. C. Bazan, T. Someya, *Adv. Mater.* **2018**, *30*, 1802359.
[3] Z. Wu, Y. Zhai, H. Kim, J. D. Azoulay, T. N. Ng, *Acc. Chem. Res.* **2018**, *51*, 3144.
[4] D. Yang, D. Ma, *Adv. Opt. Mater.* **2019**, *7*, 1800522.
[5] J. Huang, J. Lee, J. Vollbrecht, V. V. Brus, A. L. Dixon, D. X. Cao, Z. Zhu, Z. Du, H. Wang, K. Cho, G. C. Bazan, T.-Q. Nguyen, *Adv. Mater.* **2020**, *32*, 1906027.
[6] E. Georgitzikis, presented at the 2019 IISW, Snowbird Utah USA, June **2019**.
[7] L. T. Chee, H. Mohseni, *Nanophotonics* **2018**, *7*, 169.
[8] D. Olmeda, C. Hilario, A. de la Escalera, J. M. Armingol, in *Advanced Concepts for Intelligent Vision Systems. ACIVS 2008*, Lecture Notes in Computer Science, vol. *5259*, Springer, Berlin/Heidelberg, Germany **2008**, pp. 958–969.
[9] D. P. Ariana, R. Lu, *J. Food Eng.* **2010**, *96*, 583.
[10] A. M. Gorbach, J. D. Heiss, L. Kopylev, E. H. Oldfield, *J. Neurosurg.* **2004**, *101*, 960.
[11] F. P. García de Arquer, A. Armin, P. Meredith, E. H. Sargent, *Nat. Rev. Mater.* **2017**, *2*, 16100.
[12] A. Rogalski, *Opto-Electron. Rev.* **2012**, *20*, 279.
[13] H. Chih-Cheng, W. Chung-Yu, J. Far-Wen, S. Tai-Ping, *IEEE Trans. Circuits Syst. Video Technol.* **1997**, *7*, 594.
[14] L. Shen, Y. Zhang, Y. Bai, X. Zheng, Q. Wang, J. Huang, *Nanoscale* **2016**, *8*, 12990.
[15] M. Kaltenbrunner, M. S. White, E. D. Głowacki, T. Sekitani, T. Someya, N. S. Sariciftci, S. Bauer, *Nat. Commun.* **2012**, *3*, 770.
[16] F. Verstraeten, S. Gielen, P. Verstappen, J. Kesters, E. Georgitzikis, J. Raymakers, D. Cheyns, P. Malinowski, M. Daenen, L. Lutsen, K. Vandewal, W. Maes, *J. Mater. Chem. C* **2018**, *6*, 11645.
[17] X. Liu, Y. Lin, Y. Liao, J. Wu, Y. Zheng, *J. Mater. Chem. C* **2018**, *6*, 3499.
[18] A. E. London, L. Huang, B. A. Zhang, M. B. Oviedo, J. Tropp, W. Yao, Z. Wu, B. M. Wong, T. N. Ng, J. D. Azoulay, *Polym. Chem.* **2017**, *8*, 2922.
[19] J. Han, D. Yang, D. Ma, W. Qiao, Z. Y. Wang, *Adv. Opt. Mater.* **2018**, *6*, 1800038.
[20] Z. Wu, Y. Zhai, W. Yao, N. Eedugurala, S. Zhang, L. Huang, X. Gu, J. D. Azoulay, T. N. Ng, *Adv. Funct. Mater.* **2018**, *28*, 1805738.
[21] C. Kaiser, K. S. Schellhammer, J. Benduhn, B. Siegmund, M. Tropiano, J. Kublitski, D. Spoltore, M. Panhans, O. Zeika, F. Ortmann, P. Meredith, A. Armin, K. Vandewal, *Chem. Mater.* **2019**, *31*, 9325.
[22] K.-J. Baeg, M. Binda, D. Natali, M. Caironi, Y.-Y. Noh, *Adv. Mater.* **2013**, *25*, 4267.
[23] Z. Wu, W. Yao, A. E. London, J. D. Azoulay, T. N. Ng, *Adv. Funct. Mater.* **2018**, *28*, 1800391.
[24] T. Hasegawa, M. Ashizawa, J. Hiyoshi, S. Kawauchi, J. Mei, Z. Bao, H. Matsumoto, *Polym. Chem.* **2016**, *7*, 1181.
[25] J. Fan, J. D. Yuen, M. Wang, J. Seifter, J.-H. Seo, A. R. Mohebbi, D. Zakhidov, A. Heeger, F. Wudl, *Adv. Mater.* **2012**, *24*, 2186.
[26] T. T. Steckler, P. Henriksson, S. Mollinger, A. Lundin, A. Salleo, M. R. Andersson, *J. Am. Chem. Soc.* **2014**, *136*, 1190.
[27] G. Simone, M. J. Dyson, C. H. L. Weijtens, S. C. J. Meskers, R. Coehoorn, R. A. J. Janssen, G. H. Gelinck, *Adv. Opt. Mater.* **2020**, *8*, 1901568.
[28] G. Simone, M. J. Dyson, S. C. J. Meskers, R. A. J. Janssen, G. H. Gelinck, *Adv. Funct. Mater.* **2019**, 1904205.
[29] M. Kielar, O. Dhez, G. Pecastaings, A. Curutchet, L. Hirsch, *Sci. Rep.* **2016**, *6*, 39201.
[30] N. C. Giebink, G. P. Wiederrecht, M. R. Wasielewski, S. R. Forrest, *Phys. Rev. B* **2010**, *82*, 155305.
[31] A. H. Fallahpour, S. Kienitz, P. Lugli, *IEEE Trans. Electron Devices* **2017**, *64*, 2649.
[32] A. Cuevas, *Energy Procedia* **2014**, *55*, 53.
[33] K. Tvingstedt, C. Deibel, *Adv. Energy Mater.* **2016**, *6*, 1502230.
[34] S. Xiong, L. Li, F. Qin, L. Mao, B. Luo, Y. Jiang, Z. Li, J. Huang, Y. Zhou, *ACS Appl. Mater. Interfaces* **2017**, *9*, 9176.
[35] A. Armin, R. D. Jansen-van Vuuren, N. Kopidakis, P. L. Burn, P. Meredith, *Nat. Commun.* **2015**, *6*, 6343.
[36] Y. Zheng, A. Fischer, N. Sergeeva, S. Reineke, S. C. B. Mannsfeld, *Org. Electron.* **2019**, *65*, 82.
[37] A. Armin, M. Hambsch, I. K. Kim, P. L. Burn, P. Meredith, E. B. Namdas, *Laser Photonics Rev.* **2014**, *8*, 924.
[38] K. Vandewal, K. Tvingstedt, A. Gadisa, O. Inganäs, J. V. Manca, *Phys. Rev. B* **2010**, *81*, 125204.
[39] F. Verstraeten, S. Gielen, P. Verstappen, J. Raymakers, H. Penxten, L. Lutsen, K. Vandewal, W. Maes, *J. Mater. Chem. C* **2020**, *8*, 10098.
[40] J. Benduhn, K. Tvingstedt, F. Piersimoni, S. Ullbrich, Y. Fan, M. Tropiano, K. A. McGarry, O. Zeika, M. K. Riede, C. J. Douglas, S. Barlow, S. R. Marder, D. Neher, D. Spoltore, K. Vandewal, *Nat. Energy* **2017**, *2*, 17053.

© 2020 The Authors. Advanced Materials published by Wiley-VCH GmbH

[41] Y. Fang, A. Armin, P. Meredith, J. Huang, *Nat. Photonics* **2019**, *13*, 1.
[42] S. M. Sze, K. K. Ng, *Physics of Semiconductor Devices*, 3rd ed., Wiley, New York **2006**.
[43] X. Hu, K. Wang, C. Liu, T. Meng, Y. Dong, S. Liu, F. Huang, X. Gong, Y. Cao, *J. Mater. Chem.* **2014**, *2*, 9592.
[44] S. Ullbrich, J. Benduhn, X. Jia, V. C. Nikolis, K. Tvingstedt, F. Piersimoni, S. Roland, Y. Liu, J. Wu, A. Fischer, D. Neher, S. Reineke, D. Spoltore, K. Vandewal, *Nat. Mater.* **2019**, *18*, 459.
[45] M. Azzouzi, J. Yan, T. Kirchartz, K. Liu, J. Wang, H. Wu, J. Nelson, *Phys. Rev. X* **2018**, *8*, 031055.
[46] K. D. Rosenthal, M. P. Hughes, B. R. Luginbuhl, N. A. Ran, A. Karki, S.-J. Ko, H. Hu, M. Wang, H. Ade, T.-Q. Nguyen, *Adv. Energy Mater.* **2019**, *9*, 1901077.
[47] Thorlabs, Calibrated Photodiodes, https://www.thorlabs.com/newgrouppage9.cfm?objectgroup_id=2822 (accessed: May 2020).
[48] Z. Wu, N. Li, N. Eedugurala, J. D. Azoulay, D.-S. Leem, T. N. Ng, *npj Flex. Electron.* **2020**, *4*, 6.
[49] K. Zhou, Y. Liu, A. Alotaibi, J. Yuan, C. Jiang, J. Xin, X. Liu, B. A. Collins, F. Zhang, W. Ma, *ACS Energy Lett.* **2020**, *5*, 589.
[50] M. Azzouzi, T. Kirchartz, J. Nelson, *Trends Chem.* **2019**, *1*, 49.
[51] A. Wadsworth, M. Moser, A. Marks, M. S. Little, N. Gasparini, C. J. Brabec, D. Baran, I. McCulloch, *Chem. Soc. Rev.* **2019**, *48*, 1596.

© 2020 The Authors. Advanced Materials published by Wiley-VCH GmbH